

Supporting Information

**Fabrication and Replication of Arrays of Single- or Multi-Component Nanostructures by
Replica Molding and Mechanical Sectioning**

Darren J. Lipomi,¹ Mikhail A. Kats,^{2§} Philseok Kim,^{1,2§} Sung H. Kang,² Joanna Aizenberg,^{1,2}
Federico Capasso,² and George M. Whitesides^{1*}

¹*Department of Chemistry and Chemical Biology, Harvard University, 12 Oxford Street,
Cambridge, MA, 02138*

²*School of Engineering and Applied Sciences, Harvard University, 29 Oxford Street, Cambridge,
MA, 02138*

[§]These authors contributed equally to this work.

*Author to whom correspondence should be addressed.

1. Mastering, Molding, Embedding, and Sectioning

Mastering and Molding. Silicon masters of the micropost and nanopost arrays were fabricated using electron-beam lithography (EBL) followed by the Bosch DRIE process as described elsewhere.¹ The surfaces of the masters were passivated with heptadecafluoro-1,1,2,2-tetrahydrodecyltrichlorosilane by exposure to a vapor. The elastomeric mold (a negative replica) of this master structure was prepared by pouring a mixed and degassed elastomer, poly(dimethylsiloxane) (PDMS, Dow-Corning Sylgard 184, mixed in a ratio of 10:1 base to hardener), over the mold. The mold was cured for 2 h at 70 °C, after which the mold was cut from the master with a razor blade. Figure S1 shows photographs of structures used during the process of molding and embedding. Figure S1a is a photograph of a PDMS mold. To form an epoxy replica, a UV-curable, single-component, epoxy prepolymer, UVO-114 (Epoxy Technology, Billerica, MA), was poured over the mold and placed in a vacuum desiccator and degassed for ~ 1 min to infiltrate the prepolymer into the mold. We poured the prepolymer so that the liquid rose above the surface of the mold by about 2 mm. This material provided a rigid backing after curing. The prepolymer was cured by irradiation with UV light (~ 100 W, with an i-line bandpass filter) for 20 min. The epoxy replica was released from the mold after cooling to room temperature (Figure S1b). These substrates were coated by evaporation, sputtering, electrochemical deposition, or drop-casting, in a manner that depended on the desired geometry and composition of the final structure. Details of specific procedures for producing structures shown in Figures 2, 3, and 4 are written in the following sections. Epoxy substrates coated with thin films (S1c) were cut into ~ 1-mm-wide strips (S1d) with a razor blade and a hammer, which were again cut into 1-mm squares (S1e). These pieces were placed, face-up, on a scrap of PDMS and treated with a brief exposure to an air plasma (5 s, 100 W, 500 mtorr, SPI Plasma Prep II),

covered with an epoxy prepolymer, and degassed in a vacuum desiccator, such that the epoxy prepolymer infiltrated the spaces between nanoposts (S1f). Separately, PDMS block molds were prepared by casting a 1-cm-thick slab of PDMS in a Petri dish and cutting the PDMS into squares. We cut a square hole ($\sim 0.5 \text{ cm} \times 0.5 \text{ cm} \times 1 \text{ cm}$, S1g) into each square of PDMS. The squares of epoxy nanoposts coated with thin films were transferred, face-down, along with a coating of uncured epoxy prepolymer, to flat pieces of PDMS (S1h). The epoxy was cured with UV light for at least 20 min; this action glued the epoxy squares to the PDMS substrates. The PDMS block molds were placed over the epoxy squares. The block molds formed a reversible seal to the PDMS substrates (S1j). The molds were filled with additional epoxy prepolymer (S1k) and again cured under UV radiation, for 20 min. The substrates were inverted and irradiated a third time, in order to ensure complete curing of the epoxy in between the nanoposts. The block molds were disassembled and the epoxy blocks containing the arrays of epoxy nanoposts were removed (S1l). Figure S2 is a schematic diagram of the process used to embed coated epoxy nanoposts so that the plane defined by the array of nanoposts was parallel with the plane of the facet of the epoxy block.

The epoxy blocks were mounted in the sample chuck of the ultramicrotome (Leica Ultracut UCT) and trimmed with a razor blade to define an area of $\sim 1 \text{ mm}^2$ around the array of embedded nanoposts. The facets of the blocks were aligned under the stereomicroscope of the ultramicrotome so that they were parallel to the edge of the knife. The tops of the nanoposts were beneath the surface of the facet of the block by $1 - 5 \text{ }\mu\text{m}$. The material produced blank slabs of epoxy. The point at which the knife cut off the tops of the nanoposts, which were covered in gold, signaled the position in the block where useable sections containing nanostructures would be cut. The blocks were sectioned at a speed of 1 mm/s with a typical set thickness of 100 nm

and collected by surface tension in a loop tool and placed on pieces of an Si wafer for imaging, or on a ZnSe window (ISP Optics) for optical characterization. Figure S3a is a photograph of a Leica UC6 ultramicrotome, which is similar to the one we used. Figure S3b is a side view of the sample chuck and knife holder as the epoxy block impinges upon the knife. Figure S3c is top view of the same action. The single-crystalline diamond blade and the water-filled trough are visible.

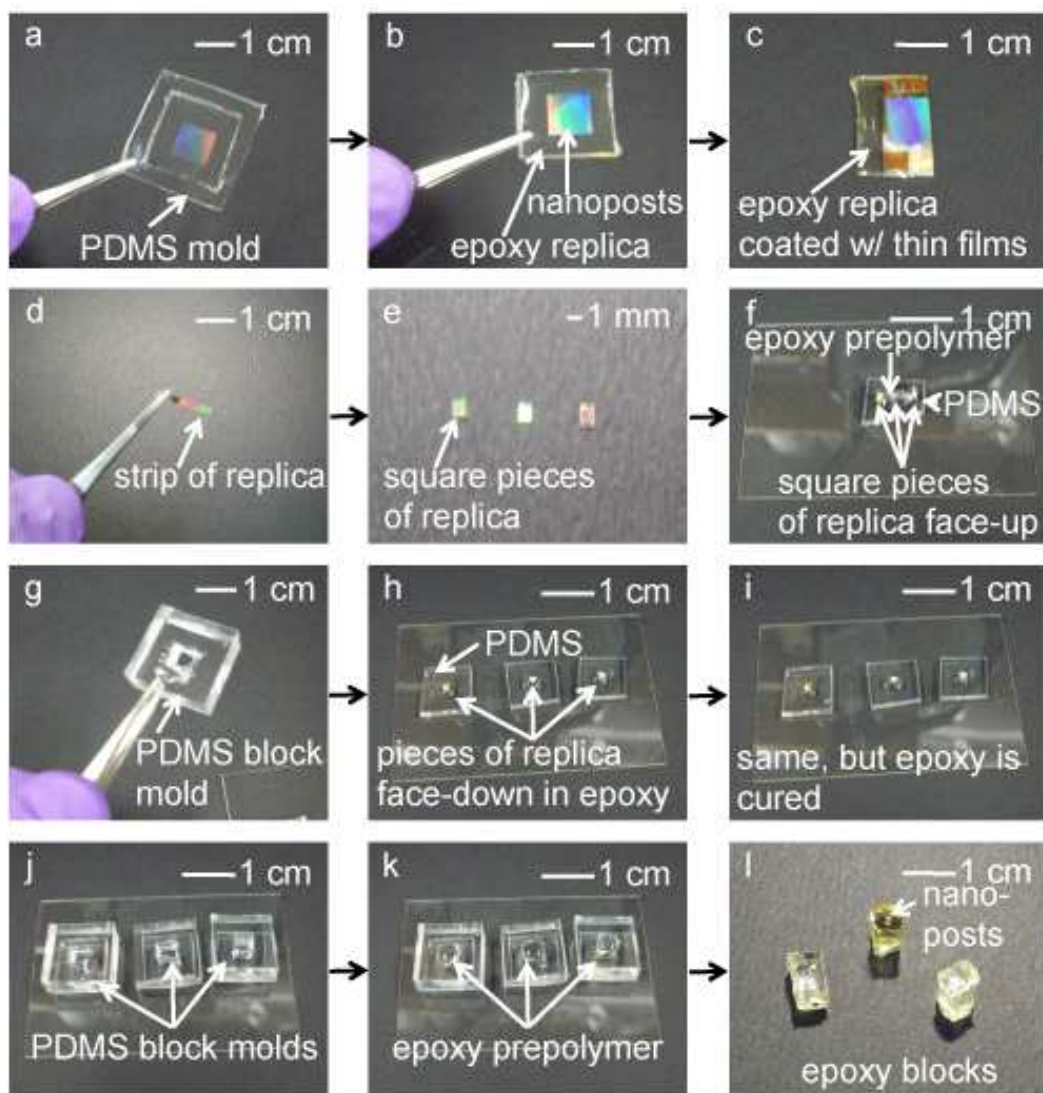


Figure S1. Photographs of structures used for molding and embedding.

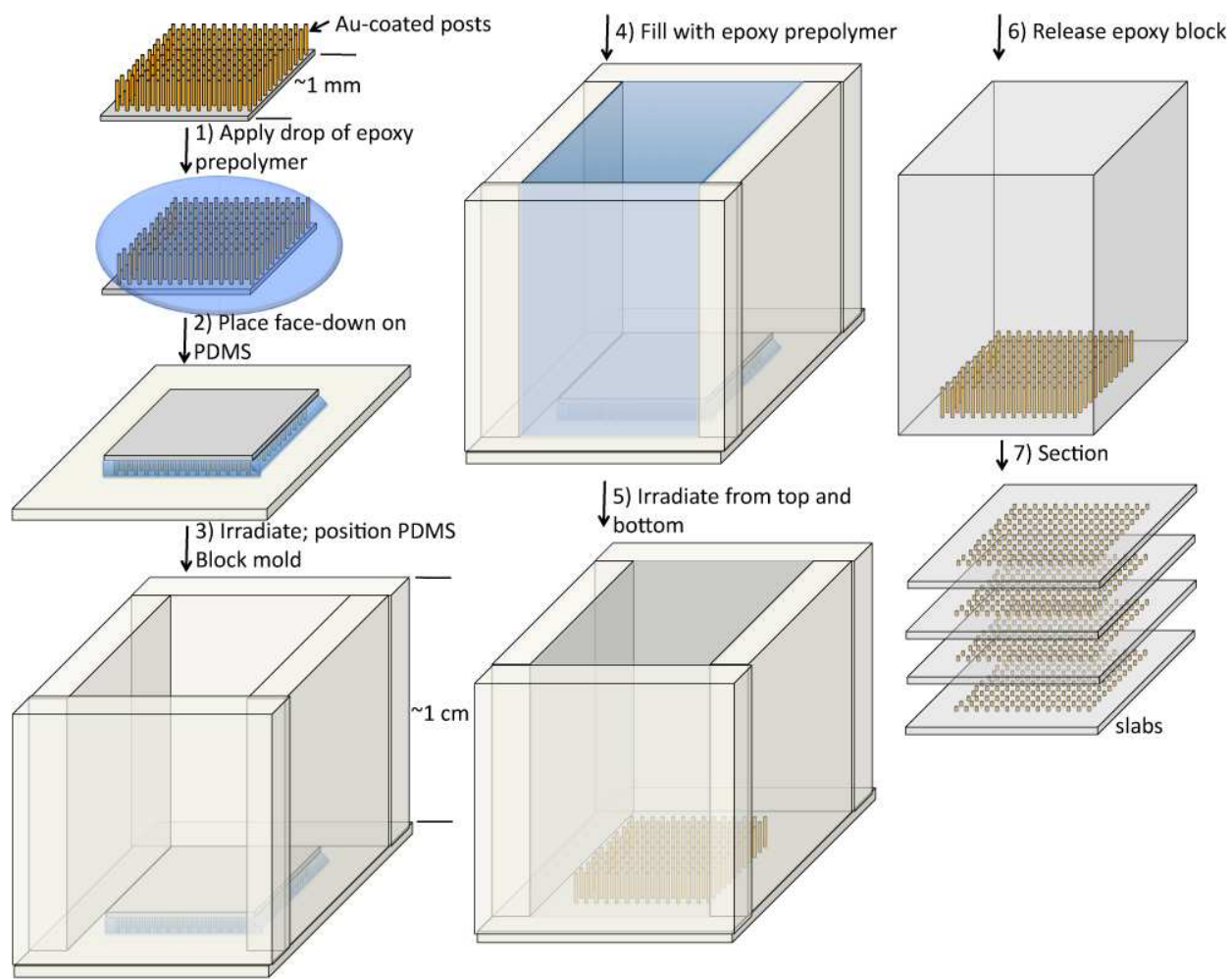


Figure S2. Schematic drawing of the process used to embed epoxy nanoparticles in epoxy so that the epoxy nanoparticles are parallel to the surface.

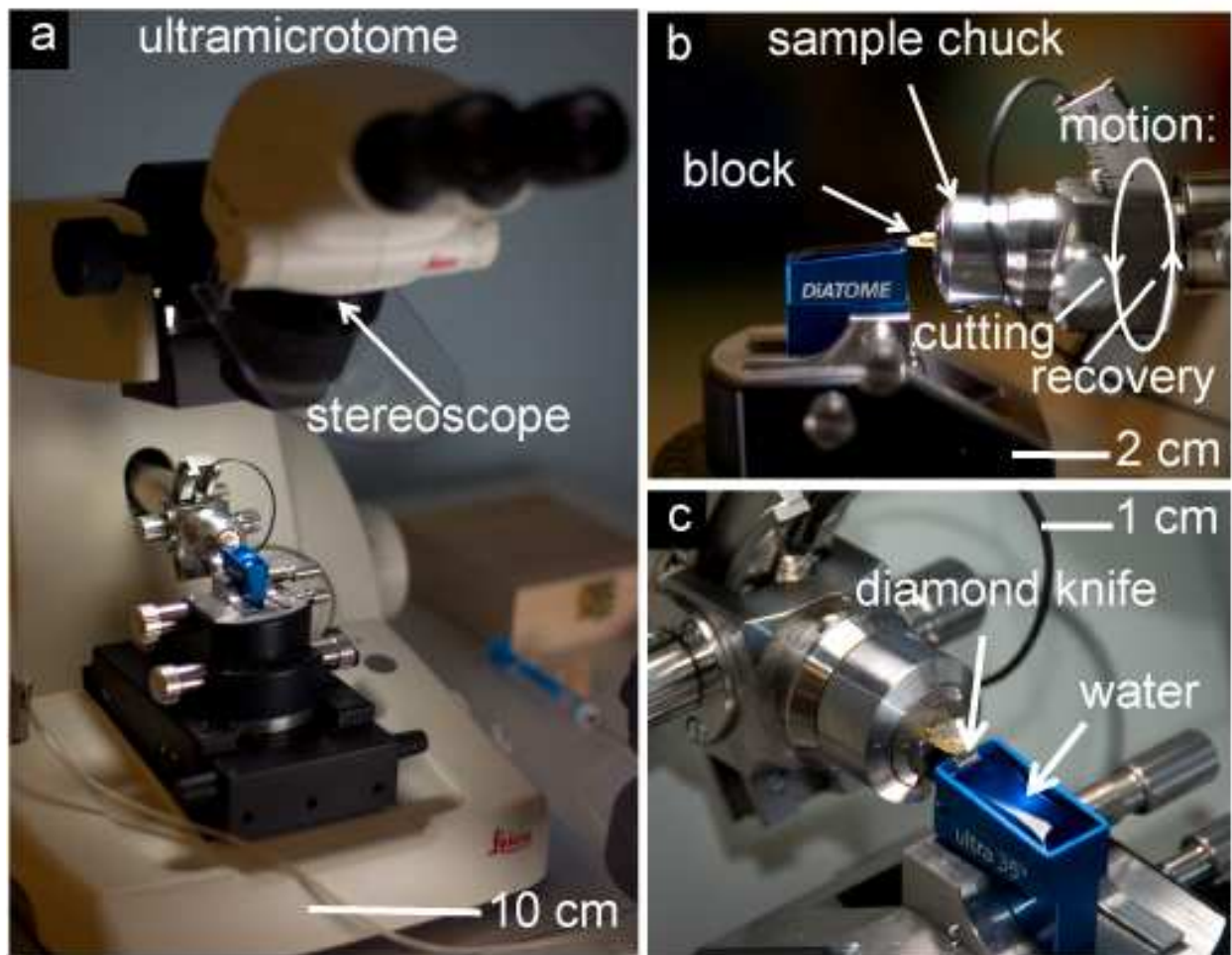


Figure S3. Photographs and schematic drawings of the tools of ultramicrotomy and nanoskiving. Images courtesy of Dr. Ryan C. Chiechi.

2. Procedures for Depositing Thin Films for Structures Shown in Figures 2, 3, and 4.

Fabrication of Single Gold Rings (Figure 2d). The epoxy replica was coated with gold at using a bench-top sputter-coater (Model 208HR, Cressington, Watford, UK) at 20 mA for 1000 s while rotating and tilting the epoxy replica. The substrate was trimmed, embedded, and sectioned, as described in the previous part.

Fabrication of Double Gold Rings (Figure 2e and 2f). A gold-coated array of epoxy nanoposts, described in the previous paragraph, was cleaned by 100 W oxygen plasma (Model

Femto, Diener GmbH, Nagold, Germany) for 10 s. Separately, we prepared a solution for electrochemical growth of polypyrrole (PPy), which contained 0.1 M pyrrole (obtained from Sigma-Aldrich, purified using an alumina column) and 0.1 M sodium dodecylbenzene sulfonate (Sigma-Aldrich). The solution was purged by dry nitrogen for 10 min. We added the gold-coated array of nanoposts to this solution. The array served as the working electrode in a standard three-electrode configuration. An anodic potential of +0.55 V vs. Ag/AgCl (saturated with NaCl) was applied potentiostatically and a platinum mesh was used as a counter electrode. The rate of growth was ~ 0.5 nm/s. Withdrawing the sample at a constant rate during the deposition produced an array with a gradient of separation between the two gold layers. The freshly deposited PPy layer was treated by applying a reductive potential of -0.5 V for 60 s. This treatment reduced the roughness (rms) of the PPy layer from 4.5 nm to 3.0 nm (scan area: $2 \mu\text{m} \times 2 \mu\text{m}$). Finally, we washed the deposited PPy layer with deionized water and dried with a stream of compressed air. We deposited the second gold layer (the outer ring) on the electrochemically deposited PPy using the same sputtering method described above, except that we used a time of deposition of 1500 s, to form a continuous film over the PPy, which was rougher than the original surface of the epoxy nanopost (the longer time of deposition filled in some of the gaps in coverage caused by the roughness of the PPy layer). Embedding and sectioning this substrate produced arrays of concentric rings separated by a spacer layer of PPy embedded in a slab of epoxy (Figure 2e). Etching the epoxy and the PPy in an air plasma (1 torr, 100 W, 10 min) produced free-standing concentric rings (Figure 2f).

Fabrication of Gold Crescents (Figure 3a). We used e-beam evaporation to deposit gold only partially around the perimeters of the nanoposts. We loaded the array of epoxy nanoposts in the chamber directly over the crucible (distance of 40 cm) at an angle of 45° and

evaporated a nominal thickness of 50 nm, as determined by the quartz crystal microbalance (QCM) detector. We embedded, sectioned, and etched this array, as before.

Fabrication of Gold Split Rings (Figure 3b). To deposit gold around most of the circumference of the epoxy posts, we performed three evaporations, and rotated the substrate by approximately 80° between each one. We deposited nominal thicknesses of 30 nm. We embedded, sectioned, and etched this array, as before.

Fabrication of Counterfacing Split Rings of Gold (Figure 3c). Starting with the array of nanoposts from which we derived single split ring, we electrochemically deposited polypyrrole on the partially gold-coated cylinder, and performed a second step of three e-beam evaporations 180° to the first. We embedded, sectioned, and etched this array, as before.

Fabrication of High-Aspect-Ratio Concentric Rings of Gold (Figure 3d and 3e). We fabricated this structure the same way as we fabricated the concentric rings, except that we obtained sections 600 nm thick. We etched this array using a long exposure to an air plasma (1 torr, 100 W, 30 min).

Fabrication of Platinum Crescents (Figure 4a). We fabricated arrays of platinum crescents using the same procedure as for the gold crescents, except that we evaporated platinum instead of gold.

Fabrication of Silver/Silicon Counterfacing Crescents (Figure 4b). We fabricated this structure by performing two evaporations. First, we evaporated silver, and then rotated the substrate by 180° , and then evaporated silicon. We did not etch the epoxy in this case because silver is sensitive to oxidation.

Fabrication of Three-Layer Crescents of Gold, SiO₂, and Pd (Figure 4c). We performed three successive evaporations without rotating the substrate within the chamber. The structure was embedded, sectioned, and etched, as before.

Fabrication of Arrays of Rings of PbS Nanocrystals (Figure 4d). We prepared a solution of PbS nanocrystals in hexanes by a reported procedure at a concentration of approximately 10^{16} nanocrystals/L.²

Measurement and Simulation of Arrays of Rings and Concentric Rings.

We transferred arrays of single and double rings to a 1-mm thick chemically vapor deposited ZnSe window (ISP Optics) for optical characterization. We etched the epoxy slab using an air plasma (1 torr, 100 W, 10 min). We covered the entire substrate except for a window around the array by drilling a circular aperture ($d = 400 \mu\text{m}$) in copper tape, and placing the hole over the array. We measured the transmission spectrum through the array. We performed transmission measurements by placing the sample at the focus of a mid-IR polarized, incoherent beam from a globar inside of the sample compartment of a Bruker Vertex 80V Fourier Transform Infrared (FTIR) spectrometer. The polarization was set to be perpendicular the direction of compression of the sample. The signal was obtained using a Deuterated Triglycine Sulfate (DTGS) detector with a resolution of 16 cm^{-1} and a mirror scanning velocity of 1.6 kHz. The sample compartment was placed under vacuum to remove any water absorption lines in the spectrum. Because the signal measured by the DGTS detector was somewhat weak, we averaged 2000 scans per spectrum for every sample. Averaging provided clean data in the range of wavelengths of 1.5 – 6 μm . For each sample, we normalized the data with a reference spectrum taken through a ZnSe substrate by covering a blank area of the ZnSe substrate with a circular aperture ($d \sim 400 \mu\text{m}$) drilled into the copper tape (transmission spectrum = raw sample spectrum / reference spectrum).

We performed all simulations using the finite difference time domain (FDTD) method using commercial FDTD software (Lumerical Solutions). We performed high resolution 3D simulations using a broadband linearly polarized plane wave source in total field - scattered field (TFSF) mode to remove the effect of the limited simulation size. Perfectly matched layers (PML) served as boundary conditions. A graded mesh was used, designed to discretize accurately the geometries of the rings. We defined the smaller ring with a resolution of < 3 nm in the plane of the ring, the large ring with a resolution of < 4.5 nm, and the free space/substrate with a resolution of < 20 nm. The vertical resolution of the rings was 3 nm. The mesh resolution was enforced to change by at most a factor of 1.4 per mesh cell. The highly dispersive complex dielectric function of gold was approximated by a three-coefficient polynomial fit of data from Palik³ over the range of wavelengths of $1.5 \mu\text{m} - 6 \mu\text{m}$. The slightly dispersive dielectric function of ZnSe was approximated by a two-coefficient polynomial fit of data provided by the supplier, ISP Optics.⁴ Due to the symmetry of our structures, we were able to apply symmetric boundary conditions. The symmetry allowed us to reduce the requirement for computational resources by a factor of four.

The distances between locations in the array in the simulation were adjusted for the experimentally observed compression. That is, the arrays were rectangular, and the axis in the direction of cutting was shorter than the uncompressed axis by 8%. However, the shapes of the rings were not adjusted for the compression found in the experimental structures (where the rings were slightly elliptical) in the simulations (we used circular rings). This discrepancy is probably the greatest source of deviation between the experimental and simulated data.

Because of the finite size of the array, and because the exact ring size, shape, and position differed slightly from unit cell to unit cell in our fabricated structures, we did not expect to see

narrow array resonances corresponding to the photonic modes of the grating created by our array of nanostructures.⁵ However, if an infinite array of structures is simulated with periodic boundary conditions, these array resonances do appear. To decouple this photonic array resonance from the plasmonic response of the gold rings, we simulated finite arrays and used those as our basis for comparison. We found that a 5×5 array of rings was sufficient to account for the very slight near-field coupling between neighboring rings, so we used simulations of a 5×5 arrays as our benchmark. Figure S4 contains the normalized transmission through a 1×1 array, a 3×3 array, a 5×5 array, and a 7×7 array, showing that simulating an array larger than 5×5 does not add significantly to the accuracy of our simulations.

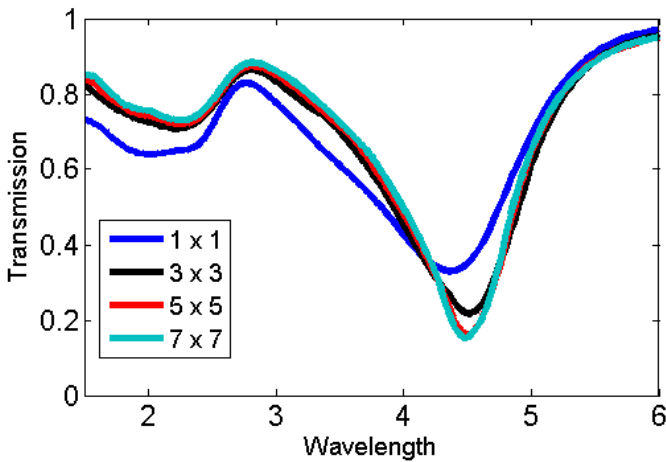


Figure S4. Simulated transmission spectra for a single set of double rings (blue), a 3×3 array (black), a 5×5 array (red), and a 7×7 array (cyan). There almost no discernable difference between the 5×5 and the 7×7 case.

Each gold ring by itself (in the absence of the other one) supports a dipole resonance at some resonant frequency. Charges on the surface of the metal move to cancel out (and reverse) the direction of the field in the vicinity of the ring. These charges also create a high field enhancement very close to the ring. Simulated field and charge profiles of the single and double ring structures from Figure 5 are plotted in Figure S5.

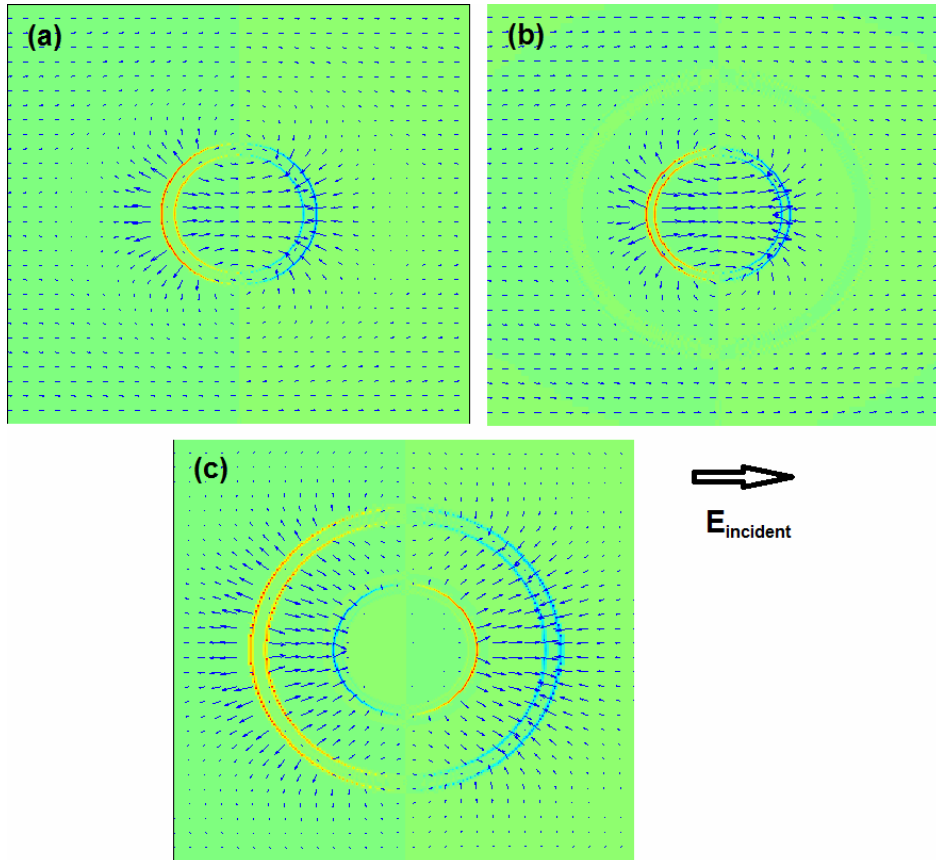


Figure S5. Simulated instantaneous electric field and charge profiles of the single ring at resonance (a), and at the lower (b) and higher (c) wavelength resonance of the double ring structure. The resonant wavelength is defined as the wavelength of lowest transmission through the array. The simulation data was monitored through the center of the ring structures. Arrows indicate the direction and magnitude of the electric field, red identifies areas of greater positive charge, while blue identifies areas of greater negative charge. Note that the charges are localized on the surfaces of the rings.

We note that the fields and charge distributions of the lower-wavelength resonance of the double ring structure (Figure S5b) are very similar to those of a dipole resonance in a single ring structures (such as one in Figure S5a). However in the higher-wavelength resonance of the double structure, the fields inside the ring encounter the inner ring and are screened, creating a charge density on the outer edge of the inner ring and nearly-zero fields inside. This interruption slightly alters the mode profile of the higher-wavelength resonance.

Fabrication of Three-Dimensional Structures and Arrays of Structures Embedded in Prism-Shaped Slabs. One of the silicon masters we used had pronounced periodic variations in the diameters of the posts (scalloping or sidewall corrugation). Epoxy replicas derived from these masters retained this trait. When sputter-coated with gold, the metal collected around the segments of the posts where the diameters were the largest. The sidewalls remained corrugated even after electrodeposition of PPy. A second metallization also deposited selectively on the wide segments of the posts. Embedding an array prepared in this way and sectioning it such that the block was angled toward the knife by $\sim 2^\circ$ produced an array with a gradient of heights, as shown in Figure 6.

Compression. Compression is an artifact of mechanical sectioning in which the slab is shorter in the direction of cutting than it is in the direction parallel to the edge of the knife. We measured a distance between sites in an array along the axis of cutting that was 8.5% shorter than in the orthogonal axis. We calculated the same value using two different batches of the same epoxy containing two different types of embedded structures. It should be possible to cancel out the effect of compression by designing masters such that the axis in the direction of cutting is elongated, so that the compression produces the desired structure. Deformation of the PDMS mold during the curing of the epoxy, for example, would generate a skewed array which could be “unskewed” by the compression.⁶ Gnaegi has shown that the use of ultrasonic, oscillating knives produces immeasurably small compression of slabs, but we have not yet used oscillating knives.⁷

Yield. Figure S6 shows an array of double rings from which yield was calculated. The array is mounted on a ZnSe crystal and contains $18 \times 27 = 486$ rings. They are 140 nm in height. There is one broken structure (labeled) and ten structures whose inner and outer rings are touching, or appear to have a metal fragment bridging the two rings (labeled).

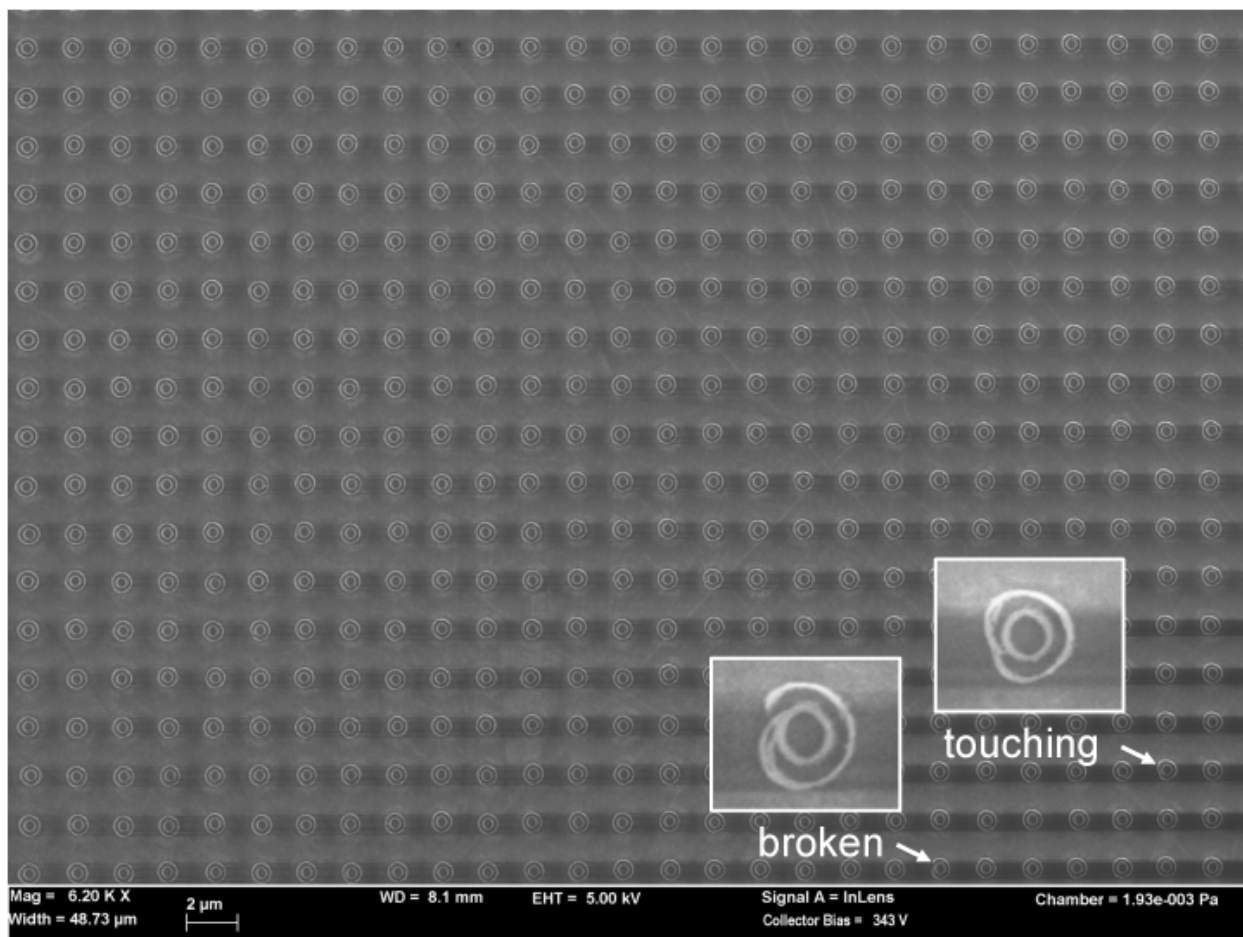


Figure S6. Array of $18 \times 27 = 486$ concentric double rings over an area of $2000 \mu\text{m}^2$.

Number of Consecutive Cross Sections. In order to determine the number of consecutive cross sections of arrays of gold rings we could obtain by repeated sectioning, we sectioned an 8- μm -tall array of gold-coated nanoposts into 100-nm slabs. We obtained 73 slabs containing contiguous arrays of at least $100 \mu\text{m} \times 100 \mu\text{m}$ in area. Figure S7 shows approximately the 10th, 20th, 30th, and 50th consecutive slab. The dark grey regions contain the arrays of gold rings; the light grey regions are blank epoxy. Two effects account for the non-uniformity of the rings across the entire area. (1) The block face was aligned to the knife by hand, and imperfect registration allowed the nanoposts on the left-hand side to section first. (2) Deformation of the array during rough cutting and embedding caused the edges to bow. This

bowing is why the area without nanostructures in the center of the right-hand side of the slab persists through the 50th slab. The 50th slab is smaller than the others, because as the knife approached the base of the posts on the left-hand side of the block, the array delaminated from the block. The probability that part of the array will delaminate increases with depth.

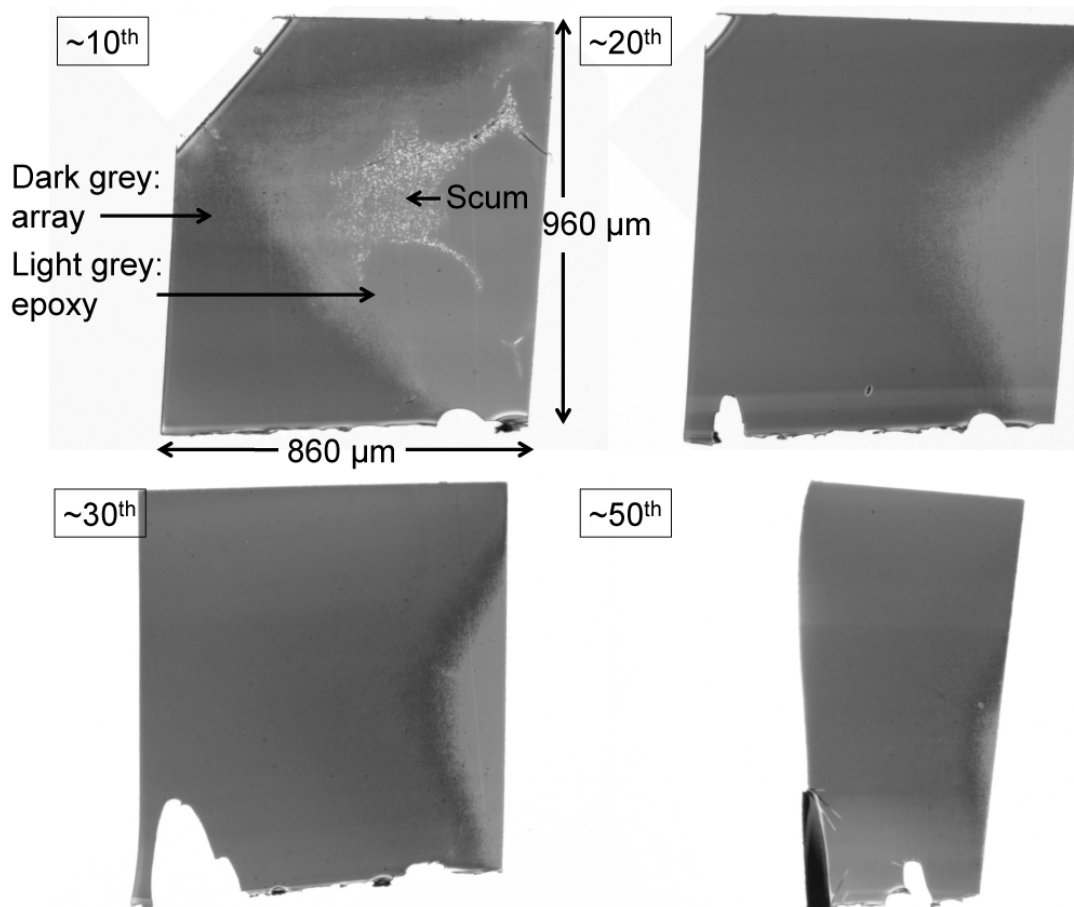


Figure S7. Images of four slabs obtained from a single array of gold-coated embedded epoxy nanoposts. The scum is residue from a droplet of water that evaporated on top of the slab.

Thinning and Thickening the Epoxy Posts. It was possible to change the diameter of the nanoposts without fabricating a new silicon master. To increase the radius, we fabricated a secondary master of epoxy, and thickened it by sputter coating metal films of controlled thickness using an AJA sputtering system. This secondary master, in turn, templated a new PDMS mold with larger diameters of pores. Epoxy replicas made from these molds had

correspondingly larger diameters. To reduce the diameters of the nanoposts, we made a different secondary master from an epoxy replica that had been thinned by plasma etching (Femto plasma cleaner, Diener electronic GmbH). PDMS molds made from these secondary masters had correspondingly smaller diameters, which templated epoxy replicas with thinner diameters.

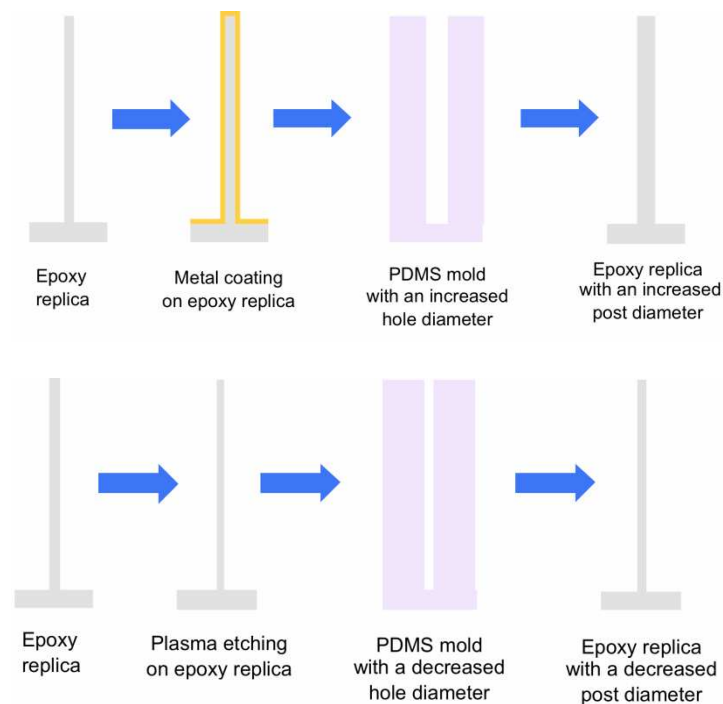


Figure S8. Summary of the procedure used to fabricate thickened and thinned epoxy posts from a single master structure.

Reducing the Scalloping from the Epoxy Posts. To reduce the scalloping of the epoxy replica, we deposited a 300 nm silver film at the deposition rate of 4 Å/s by DC sputtering (AJA sputtering system). Then, a new PDMS mold was made using the metalized replica as a master. A new replica, generated from this PDMS mold, was thinned by oxygen plasma to produce an array of epoxy posts with the desired diameters and reduced scalloping. Figure S8 shows a schematic drawing of the process used.

References

1. McAuley, S. A.; Ashraf, H.; Atabo, L.; Chambers, A.; Hall, S.; Hopkins, J.; Nicholls, G., Silicon micromachining using a high-density plasma source. *J. Phys. D, Appl. Phys.* **2001**, *34*, 2769-2774.
2. Ghadimi, A.; Cademartiri, L.; Kamp, U.; Ozin, G. A., Plasma within templates: Molding flexible nanocrystal solids into multifunctional architectures. *Nano Lett.* **2007**, *7*, 3864-3868.
3. Palik, E. D., *Handbook of Optical Constants of Solids*. Academic Press: New York, 1985.
4. ISP Optics, Optical Materials Specifications.
<http://www.ispoptics.com/OpticalMaterialsSpecs.htm> (accessed March 25).
5. Zou, S. L.; Janel, N.; Schatz, G. C., Silver nanoparticle array structures that produce remarkably narrow plasmon lineshapes. *J. Chem. Phys.* **2004**, *120*, 10871-10875.
6. Pokroy, B.; Epstein, A. K.; Persson-Gulda, M. C. M.; Aizenberg, J., Fabrication of Bioinspired Actuated Nanostructures with Arbitrary Geometry and Stiffness. *Adv. Mater.* **2009**, *21*, 463-469.
7. Studer, D.; Gnaegi, H., Minimal compression of ultrathin sections with use of an oscillating diamond knife. *J. Microsc. Oxford* **2000**, *197*, 94-100.